Figure S1. Isoprene and monoterpene surface fluxes for the DCGL scenario (a–b). Panels (c) and (d) show the spatial differences in isoprene and monoterpene emission fluxes (DCGL − PNV). Monthly emissions are based on the 10-year global averages for isoprene (e) and monoterpenes (f). The shading represents 1 standard deviation, derived from the monthly averages based on 10 simulated years. Fluxes in the Southern Hemisphere were shifted by 6 months to align with the seasonal cycle.
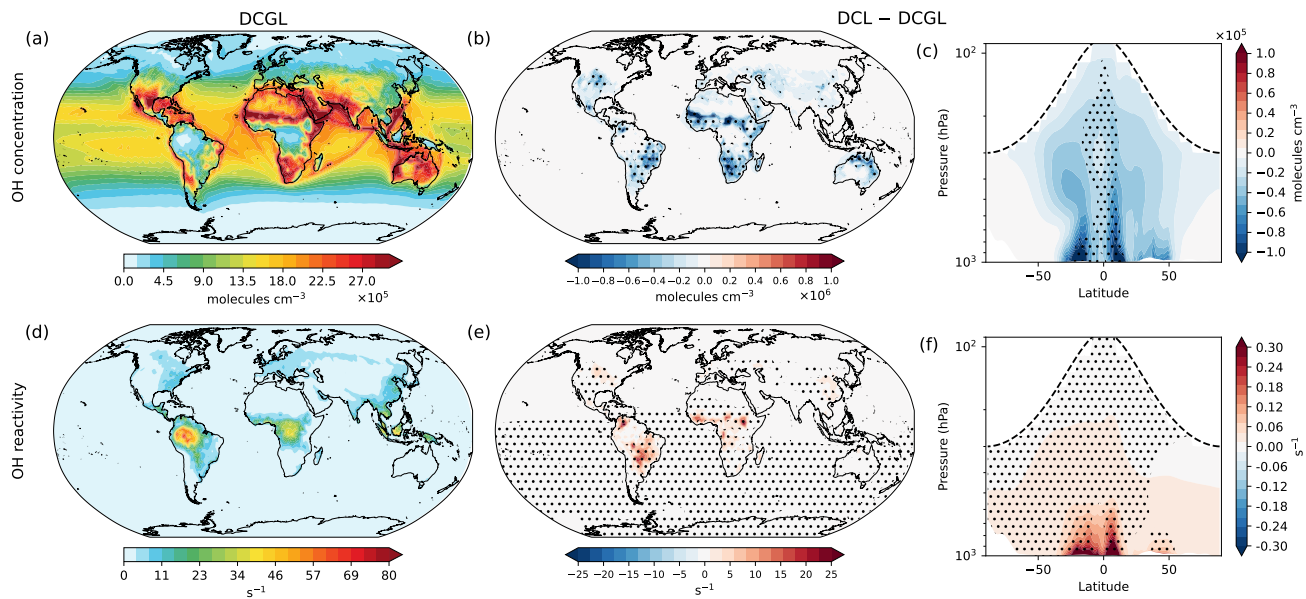
Figure S2. Shift in OH concentration and reactivity. Panels (a) and (d) display the spatial distribution of surface OH concentration and OH reactivity, respectively, under the DCGL scenario. Panels (b) and (e) depict the spatial changes at the surface (DCL − DCGL), while panels (c) and (f) show the zonal average across longitudes up to 100 hPa, highlighting OH concentration and OH reactivity changes in the troposphere, respectively. The dashed line in panels (c) and (f) represents the average tropopause height. Averages include day and night OH concentration and reactivity. Dot hatching indicates a statistically significant change based on a two-tailed Student's t-test with 95% confidence.
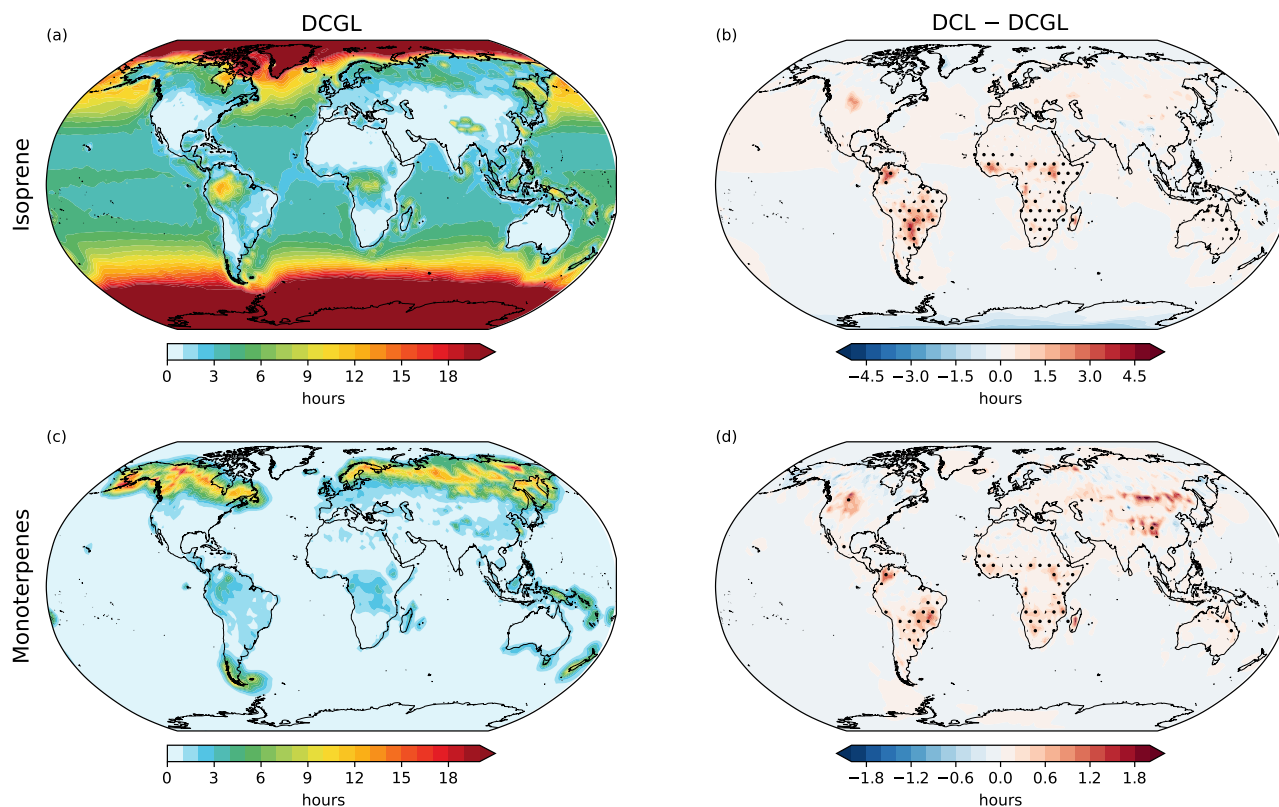
Figure S3. Spatial distribution of isoprene (a) and monoterpene (b) chemical lifetime against OH and O$_3$ oxidation at the surface. Panels b and d show the changes (DCL − DCGL) in isoprene and monoterpene lifetimes, respectively. Dot hatching indicates a statistically significant change based on a two-tailed Student's t-test with 95% confidence.
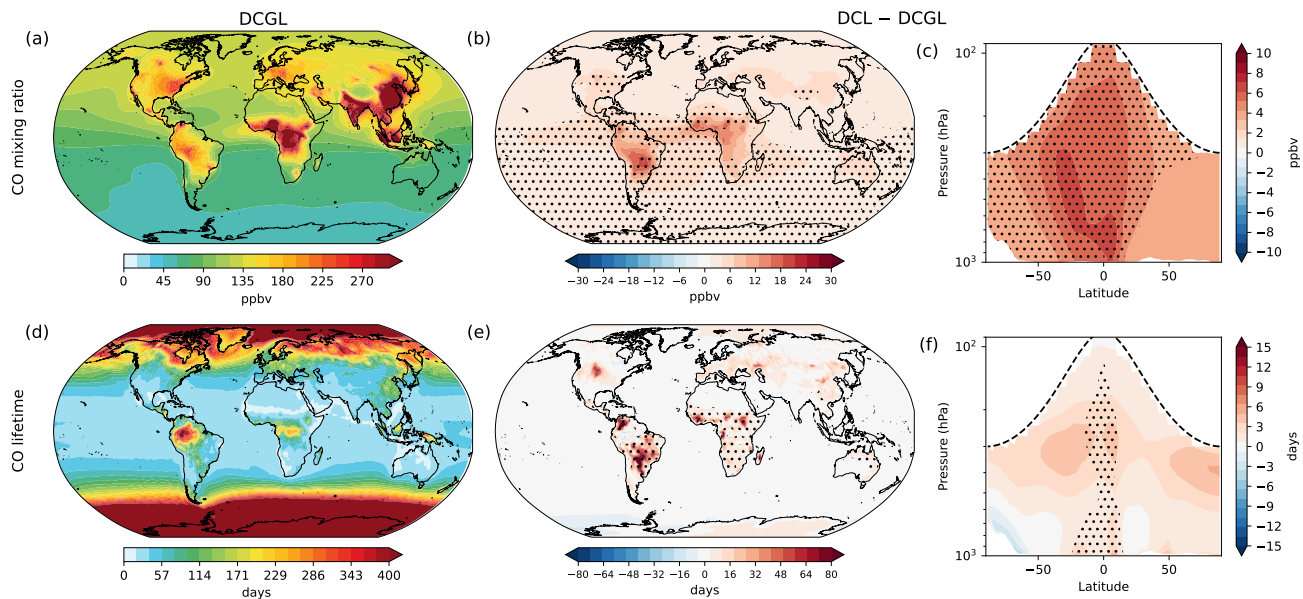
Figure S4. Changes in CO mixing ratios and lifetime. Panels (a) and (d) display the spatial distribution of surface CO mixing ratios and lifetime, respectively, under the DCL scenario. Panels (b) and (e) depict the spatial changes at the surface (DCL − DCHL), while panels (c) and (f) show the zonal average across longitudes up to 100 hPa, highlighting changes in the troposphere for CO mixing ratios and lifetime, respectively. The dashed line in panels (c) and (f) represents the average tropopause height. Dot hatching indicates a statistically significant change based on a two-tailed Student's t-test with 95% confidence.
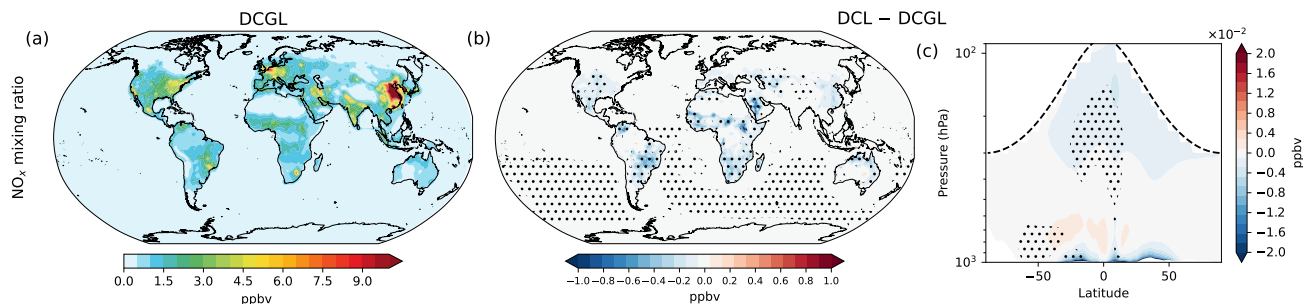
Figure S5. Same as Fig.S4a-c but for NO_x.
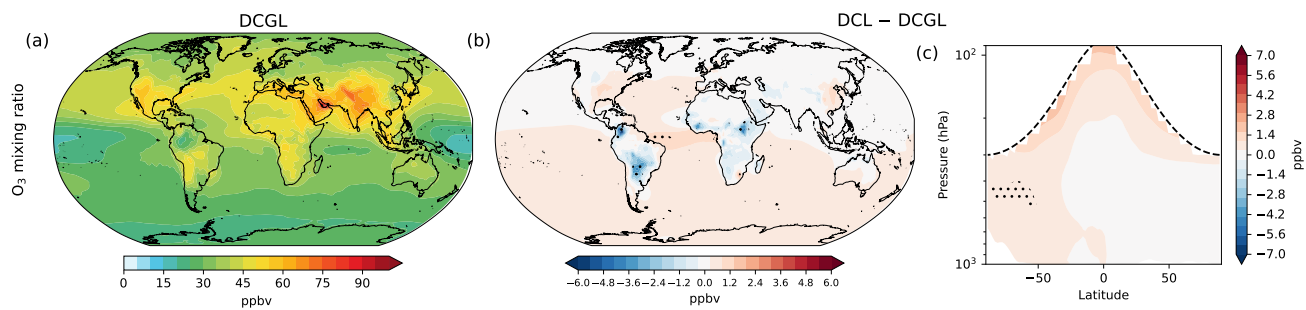
Figure S6. Same as Fig.4a-c but for O$_3$.
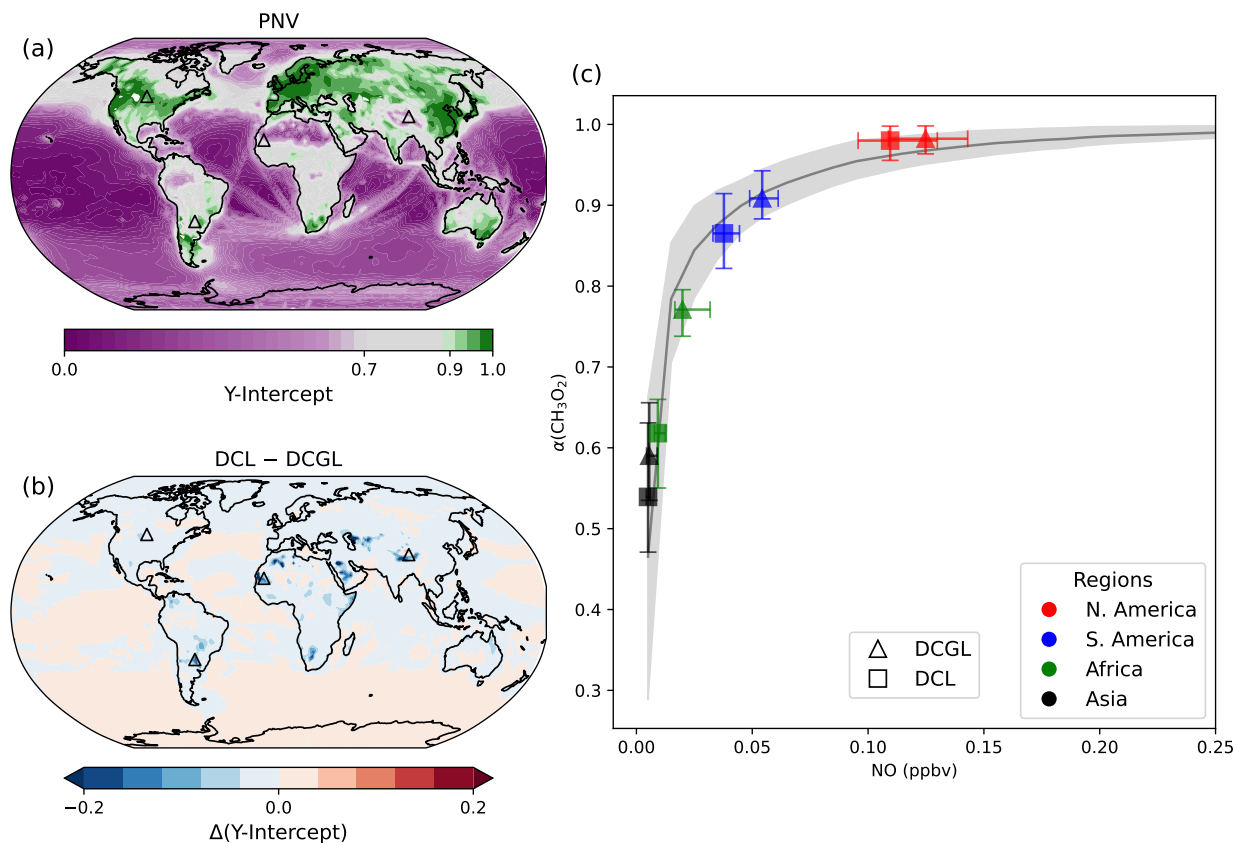
Figure S7. Changes in O_3 production sensitivity are analysed using the relationship between $\alpha(CH_3O_2)$ and NO. Panel (a) illustrates the global distribution of the y-intercept in the PNV scenario, while panel (b) displays the change in y-intercept (Δy-intercept), calculated as DCL $-$ DCGL. Panel (c) presents the medians for $\alpha(CH_3O_2)$ vs. NO, including the background curve derived from medians (computed over $2° \times 2°$ grid cells) for all data points, with 25th-75th percentile range shading. It also shows medians for North America, South America, Africa, and Asia, with the corresponding locations marked by triangle symbols in panel (b). Triangle markers represent results from the DCGL run, and square markers indicate results from the DCL run. Both markers include error bars reflecting 25th-75th percentiles.
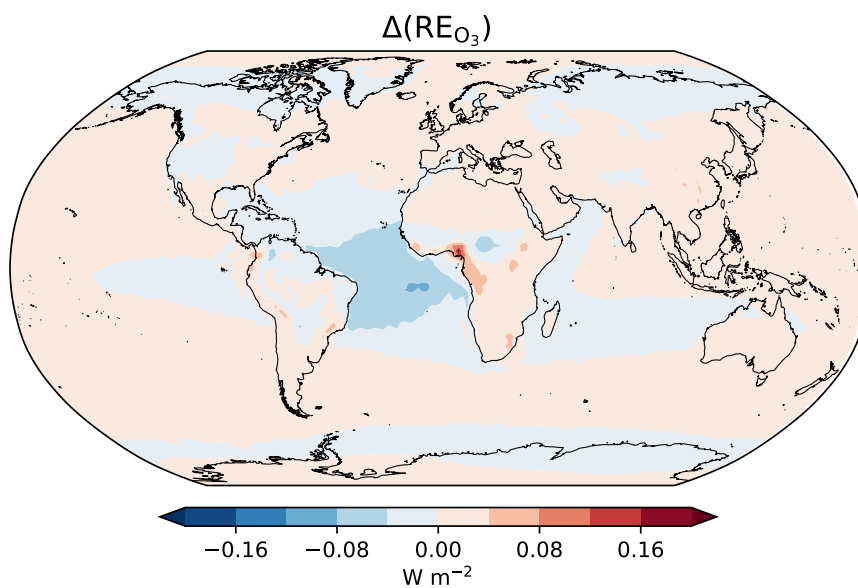
Figure S8. Radiative effects due to O_3 changes from the deforestation (DGL − DCGL) scenario, showing the top-of-the-atmosphere (TOA) radiative effect (shortwave + longwave).
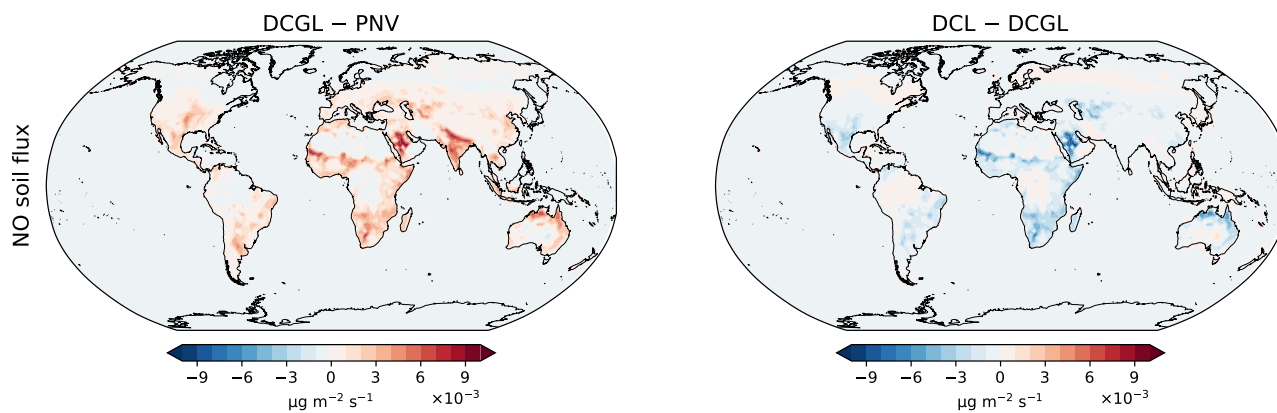
Figure S9. Soil NO emission flux changes. Panel (a) DCGL − PNV and panel (b) DCL − DCGL.
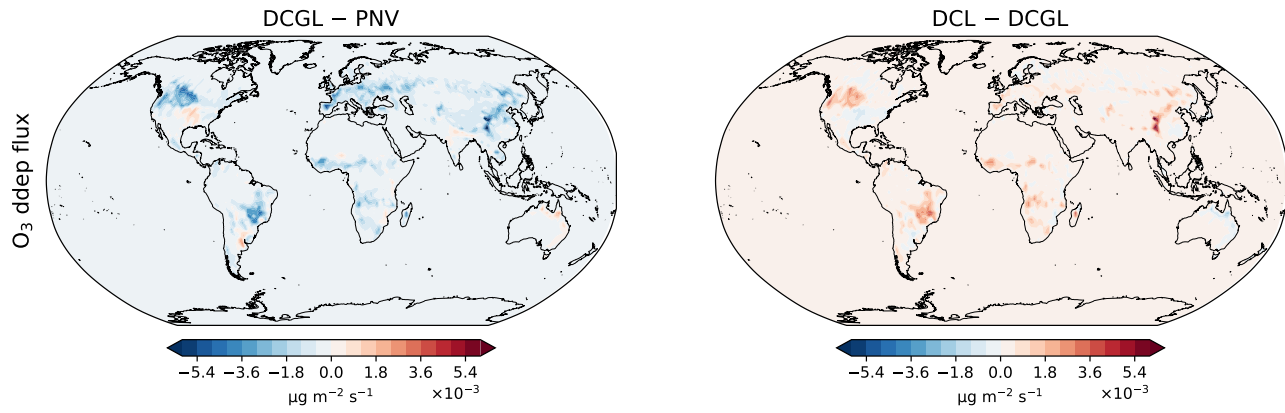
Figure S10. O_3 dry deposition flux changes. Panel (a) DCGL − PNV and panel (b) DCL − DCGL.

	PNV	**DCL**	**DCGL**
BC	3.14	3.14	3.39
OC	6.84	6.84	8.64
CO	400	400	437.1
NH_3	4.85	13.52	40.1
NO_x	58.60	58.80	61.44
SO_2	83.08	83.08	83.28

Table S1. Prescribed emissions in the different runs. Global annual means in Tg.